Phase Transitions in Magnesium Nitrate Thin Films: A Transmission FT-IR Study of the Deliquescence and Efflorescence of Nitric Acid Reacted Magnesium Oxide Interfaces

Hind A. Al-Abadleh and V. H. Grassian*

Departments of Chemistry and Chemical and Biochemical Engineering, University of Iowa, Iowa City, Iowa 52242

Received: November 26, 2002; In Final Form: June 17, 2003

In this study, transmission FT-IR spectroscopy is used to investigate the role of water in nitric acid uptake on MgO(100) and water uptake on nitric acid reacted MgO(100) at 296 K. Under dry conditions, nitric acid uptake is limited to the topmost surface layer and saturates at a nitrate coverage of $(2.3 \pm 0.1) \times 10^{15}$ ions cm^{-2} to form a single layer of magnesium nitrate. In the presence of water vapor at 25% relative humidity (RH), subsurface layers can react and the extent of nitric acid uptake and the formation of magnesium nitrate is significantly enhanced on MgO(100) without evidence of saturation. Following reaction with nitric acid, water adsorption/desorption isotherms have been measured in the presence of 0.2−20 Torr water vapor pressure corresponding to 1−95% RH on surfaces with varying nitrate coverages. The infrared spectra clearly show two phase transitions in these thin nitrate films as a function of increasing RH. One transition occurs at low relative humidity, <10% RH, corresponding to the formation of crystalline magnesium nitrate hydrates, $Mg(NO_3)_2 \cdot nH_2O$, $4 < n \leq 6$. The second phase transition occurs between 49 and 55% RH and corresponds to the deliquescence of crystalline $Mg(NO_3)_2 \cdot 6H_2O$ to an aqueous salt solution. Thinner films deliquesce at 49 ± 2% RH, whereas thicker nitrate films deliquesce at 54 ± 2% RH ,which is within experimental error of the value for pure $Mg(NO_3)_2 \cdot 6H_2O$ crystals. The efflorescence RH, i.e., crystallization as a function of decreasing RH, depends to an even greater extent on the film thickness. Thinner films of magnesium nitrate show no evidence of efflorescence whereas thicker films show efflorescence at 48 ± 3%. Atomic force microscopy (AFM) images of nitric acid reacted MgO(100) surfaces show that the surface roughness significantly increases relative to the unreacted surface. The rougher surface and the size of the features, on the order of nanometers in dimension, provide nucleation sites for crystallization to occur.

Introduction

Mineral oxide dissolution in aqueous and acidic media has a great impact in technology, environmental, and geochemical sciences.[1] Hydrometallurgy is one example of how dissolution properties of ores can be used to obtain pure metal oxides. It is well-established that the liquid/solid interface plays a role in changing the chemical properties of oxide surfaces, including ion sorption, dissolution, and catalytic activity.[2] Because surfaces of "dry" metal oxides not in contact with a liquid layer are thought to be coated with several layers of water under ambient conditions, understanding the nature of oxide surfaces and other environmental interfaces under ambient conditions is an important issue with respect to its reactivity and properties. In addition, the physicochemical properties of the oxide surface will change upon reaction with trace pollutant gases, such as HNO_3 and SO_2.

Magnesium oxide is an ideal model for ionic metal oxides because it crystallizes into the rock salt structure.[3] Importantly, from the perspective of understanding on a molecular level the structure and reactivity of the oxide surface, the most stable surface, the 100 face, can be modeled using ab initio theory.[4−6] Water adsorption on MgO(100) as a function of relative humidity at 296 K has been studied by transmission FT-IR spectroscopy.[7] There is evidence for both molecular and dissociative water adsorption on MgO(100).[7−11] Dissociative adsorption occurs at high relative humidity in the presence of a few layers of adsorbed water, suggesting a dissociative adsorption mechanism involving a cooperative effect between several water molecules and the surface.

In this study, transmission FT-IR spectroscopy is used to investigate both the heterogeneous reaction of gas-phase nitric acid on MgO(100) at 296 K under dry and wet conditions (25% RH) and water uptake on these reacted surfaces. The spectra are analyzed to obtain information about the effect of water vapor on the uptake of nitric acid on MgO(100), and, in turn, the effect of adsorbed nitrate on water uptake. Water adsorption/desorption isotherms on the nitric acid reacted surfaces are followed as a function of RH for surfaces with different nitrate coverages. As discussed in detail here, several phase transitions are identified including the transition from metastable solid magnesium nitrate and surface adsorbed water to crystalline magnesium nitrate hydrate, $Mg(NO_3)_2 \cdot nH_2O$ with $4 < n \leq 6$, and the transition from crystalline magnesium nitrate hexahydrate, $Mg(NO_3)_2 \cdot 6H_2O$, to aqueous salt solutions as a function of increasing water vapor pressure. Surface roughness measurements of reacted and unreacted surfaces have also been measured using AFM to better understand the effect of nitric acid reaction on surface topography and the role of surface roughness in the kinetics of the efflorescence process, i.e., the nucleation of crystalline magnesium nitrate hexahydrate from aqueous phase as a function of decreasing RH.

* To whom correspondence should be addressed. Tel.: +1-319-335-1392. Fax: +1-319-335-1270. E-mail address: vicki-grassian@uiowa.edu.

10.1021/jp0275692 CCC: $25.00
Published on Web 09/06/2003

Experimental Section

FT-IR spectroscopy has been employed to study the reaction of gas-phase nitric acid with MgO(100). An FT-IR spectrometer (Mattson RS-1) equipped with a liquid nitrogen cooled narrow band MCT detector was used in these studies. An infrared cell and gas handling system designed for these studies have been described previously.[12] Briefly, the gas handling system consists of a glass manifold with four ports, a gas mixing chamber and two absolute pressure transducers (MKS instruments) that operate in the range 0.001−10.00 and 0.1−1000 Torr (accuracy 0.5%). The volume of the glass manifold is 803 ± 6 mL and that of the mixing chamber is 475 ± 6 mL. The glass manifold is connected to a pumping system that includes a mechanical pump (Leybold D4A, 127 L min^{-1}) used for rough pumping and a turbo molecular pump (Alcatel, 140 L s^{-1}) used to pump the system down to a final pressure of around 10^{-6} Torr range. The gas handling system is connected to the IR cell through a Teflon tube. A cylindrical 4.8 × 5.1 cm Pyrex IR cell (volume = 122 ± 4 mL) was placed in the sample compartment of the spectrometer. Two wedged Ge windows (Janos Technology Inc.) were placed in two stainless steel holders that are O-ring sealed to the Pyrex IR cell. A Teflon holder placed inside of the infrared cell held the single crystals in place.

Dry gaseous nitric acid was taken from the vapor of a 1:3 by volume mixture of concentrated HNO_3 (70.6% HNO_3, Mallinckrodt) and H_2SO_4 (95.9%, H_2SO_4, Mallinckrodt). The water vapor was obtained from a high purity commercial water source (Fisher Scientific, Optima water). Both liquids were subjected to several cycles of freeze−pump−thaw before use. MgO(100) single-crystal surfaces were purchased from MTI Corp. A total of four 0.5 mm thick single crystals were polished on both sides. The single crystals were placed on a Teflon holder inside the IR cell and canted 45° with respect to vertical to minimize the effects of Etalon fringes.[13] The single crystals were calcined in air at 773 K for 21 h before use.

Background scans of the single-crystal surfaces were recorded before introducing the gas. All spectra shown in this study are referenced to the calcined and unreacted MgO(100) surfaces. For dry nitric acid adsorption experiments, FT-IR spectra were recorded in the presence of and after evacuation of gas-phase nitric acid. Each spectrum represents an average of 1000 scans at a resolution of 8 cm^{-1}. For wet nitric acid adsorption experiments, both gas-phase H_2O and HNO_3 were added to the mixing chamber prior to introduction to the IR cell. For water adsorption/desorption experiments, water was introduced in the infrared cell and allowed to equilibrate for at least 20 min before each spectrum was recorded. All spectra were recorded in the presence of gas-phase water as a function of water vapor pressure (0.2−20 Torr) at 296 K, corresponding to 1−95% RH. Spectra of gas-phase water and nitric acid were used to subtract out gas-phase absorptions in the presence of the sample. Each water spectrum represents an average of 100 or 250 scans at a resolution of 8 cm^{-1}. All spectra were collected in the spectral region extending from 750 to 5000 cm^{-1}.

Attenuated total reflection FT-IR (ATR FT-IR) measurements were carried out using a horizontal liquid cell ATR attachment (Pike Technologies) with a ZnSe element. Spectra of magnesium nitrate solutions and $Mg(NO_3)_2 \cdot 6H_2O$ crystals (Alfa Aesar) were collected by averaging 250 and 100 scans at 4 and 8 cm^{-1}, respectively. A similar number of scans were collected of the background ZnSe element.

Surface roughness and section analyses were measured for reacted and unreacted MgO(100) single crystals using tapping mode AFM (Digital Instruments Nanoscope III). Images were collected in air at a scan rate of 0.5 Hz. The unreacted surface was stored in a desiccator after calcining in air for several weeks before imaging. The reacted surface was imaged 1 day after experiments in the infrared cell.

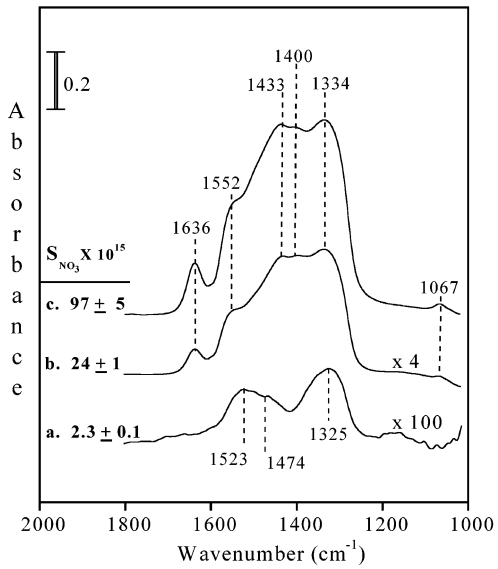

Figure 1. Transmission FT-IR spectra of MgO(100): (a) following reaction with nitric acid under dry conditions, $S_{NO_3} = (2.3 \pm 0.1) \times 10^{15}$ ions cm^{-2}; (b) following reaction under wet conditions (25% RH), S_{NO_3}, of $(2.4 \pm 0.1) \times 10^{16}$ ions cm^{-2}; (c) following additional reaction under wet conditions (25% RH), $S_{NO_3} = (9.7 \pm 0.5) \times 10^{16}$ ions cm^{-2}.

Results

1. Surface Reaction of Gas-Phase Nitric Acid on MgO(100). Eight MgO(100) surfaces were allowed to react with gas-phase nitric acid under dry and wet conditions (RH = 25%). Under dry conditions, nitrate absorption bands in the spectral range extending from 1200 to 1600 cm^{-1} grow in as a function of nitric acid pressure (35−91 mTorr). Higher pressures, up to 352 mTorr, did not result in any additional adsorption of nitric acid, as measured by FT-IR spectroscopy, indicating that the surface becomes saturated toward further reaction with gas-phase nitric acid. The spectrum shown in Figure 1a is of MgO(100) after the surface was saturated with nitric acid under dry conditions. The spectrum shows two broad absorptions that can be deconvoluted into at least three bands at 1325, 1475, and 1523 cm^{-1}, which represent a splitting of the degenerate asymmetric stretch, $\upsilon_3(E')$, of the adsorbed NO_3^- ion. The degree of splitting and relative intensities of these absorptions are sensitive to the coordination environment of the nitrate ion. For example, in the IR spectrum of crystalline magnesium nitrate dihydrate, $Mg(NO_3)_2 \cdot 2H_2O$, the nitrate ion is coordinated to the Mg^{2+} ion in a bidentate fashion.[14] The separation between the 1466 and 1330 cm^{-1} bands is 136 cm^{-1}, which is larger than that for the tetrahydrate where nitrate is monodentate coordinated. In addition, the high-frequency band at 1466 is as intense as the low-frequency band at 1330 cm^{-1} in the dihydrate, which is the opposite of what is observed for the tetrahydrate. For the amorphous anhydrous magnesium nitrate, strong absorptions at 1380 and 1475 cm^{-1} have been reported.[15] Nitrate absorptions above 1500 cm^{-1} have been observed for anhydrous beryllium nitrate owing to covalent interactions between the metal and the nitrate ion. Thus, the large degree of separation of the bands at 1325 and 1523 cm^{-1} seen in the spectrum shown in Figure 1a and the broadness of the bands suggest that reaction of nitric acid with MgO(100) surface under dry conditions results in

nitrate ion coordination that differs somewhat from either the dihydrate or the tetrahydrate nitrate salts and is representative of an amorphous form of magnesium nitrate. As will be shown in the next section, such a film is metastable and undergoes restructuring upon exposure to water vapor, forming more stable crystalline hydrate salts. The reaction can be viewed as an ion exchange reaction whereby two NO_3^- ions replace on O^{2-} ion, forming a passivating film similar to what has been observed in the dry reaction of HNO_3 with NaCl(100).[16] Such reaction occurs with little or no restructuring of the surface because, in the absence of adsorbed water, very little ionic mobility can occur.

For the reaction of HNO_3 with MgO(100) at 25% RH, the same eight surfaces were then reacted with nitric acid pressures of 10, 31, 110, and 302 mTorr, respectively, for 1 h. The resulting spectrum following the highest nitric acid pressure used and following evacuation of the gas phase for an extended period of time to remove weakly adsorbed water, are shown in Figure 1b. To obtain even higher coverages, the same four crystals were reacted further with higher pressures of nitric acid (600 mTorr for 80 min and 1.780 Torr for 1 h) at 25% RH. The final spectrum obtained following reaction and evacuation of the gas phase overnight is shown in Figure 1c. Spectra recorded of the MgO(100) surface after reaction of nitric acid under wet conditions show enhanced nitrate absorptions even though the surface had been saturated under dry conditions. Again, the υ_3 nitrate band is rather complex and contains several overlapping bands extending from 1200 to 1600 cm^{-1} near 1334, 1400, 1433, and 1552 cm^{-1}. The band at 1636 cm^{-1} is associated with strongly bound adsorbed water on the surface that is not removed under vacuum, and the band at 1067 cm^{-1} is associated with the symmetric stretching mode of the nitrate ion. Although the thicker nitrate films have some residual water associated with it, these films are metastable in nature. As shown in the next section, these metastable magnesium nitrate films undergo reconstruction to the stable crystalline hydrate solid upon exposure to water vapor. In all cases, evacuation of water from the gas phase for extended times after a cycle of water adsorption/desorption results in the formation of the nitrate metastable solid that contains some residual water.

The nitrate ion coverage can be determined from a modified form of Beer−Lambert's law:[12,13]

$$\tilde{A}/\mathrm{cm}^{-1} = \frac{NS\bar{\sigma}}{2.303 \cos 45°} \quad (1)$$

where $\tilde{A}$ is the integrated absorbance of the band of interest (cm^{-1}), $N = 8$ MgO(100) surfaces, S is the surface coverage in molecules (or ions) cm^{-2}, and $\bar{\sigma} = (4\pi/\rho) \int_{\text{band}} \kappa(\tilde{\nu})\tilde{\nu}\, d\tilde{\nu}$, where $\kappa(\tilde{\nu})$ is the wavenumber-dependent imaginary part of the index of refraction.

Although the exact details of how the integrated cross section, $\bar{\sigma}$,[17] is determined and the approximations used to calculate S_{NO_3} are given in the Discussion, the results of these calculations yield a surface coverage of nitrate ions, S_{NO_3}, of $(2.3 \pm 0.1) \times 10^{15}$ ions cm^{-2} for nitric acid reaction with MgO(100) under dry conditions. Under these dry conditions, the ratio of the nitrate coverage to the MgO ion pair density of 1.13×10^{15} ions cm^{-2} is very close to 2:1, indicating the formation of a magnesium nitrate monolayer according to

$$MgO + 2HNO_3 \rightarrow Mg(NO_3)_2 + H_2O \quad (2)$$

Quantification of the nitrate coverage for experiments done at 25% RH, yields values of $S_{NO_3} = (2.4 \pm 0.1) \times 10^{16}$ and $(9.7 \pm 0.5) \times 10^{16}$ ions cm^{-2} for reacted surfaces whose spectra are shown in Figure 1b,c, respectively. The values of the nitrate coverage determined under conditions of 25% RH are all higher than the ion pair density of the MgO(100) surface by a factor of approximately 20−100 times. Thus at 25% RH, subsurface layers of the MgO surface are reacting. Further evidence for subsurface reactant layers are evident under reaction conditions done at pressures above 302 mTorr, where there is no evidence of surface saturation after 1 h of reaction; i.e., using FT-IR analysis to monitor the nitrate absorption band as a function of time shows the nitrate absorption band increasing linearly in intensity with reaction time with no evidence of leveling off.

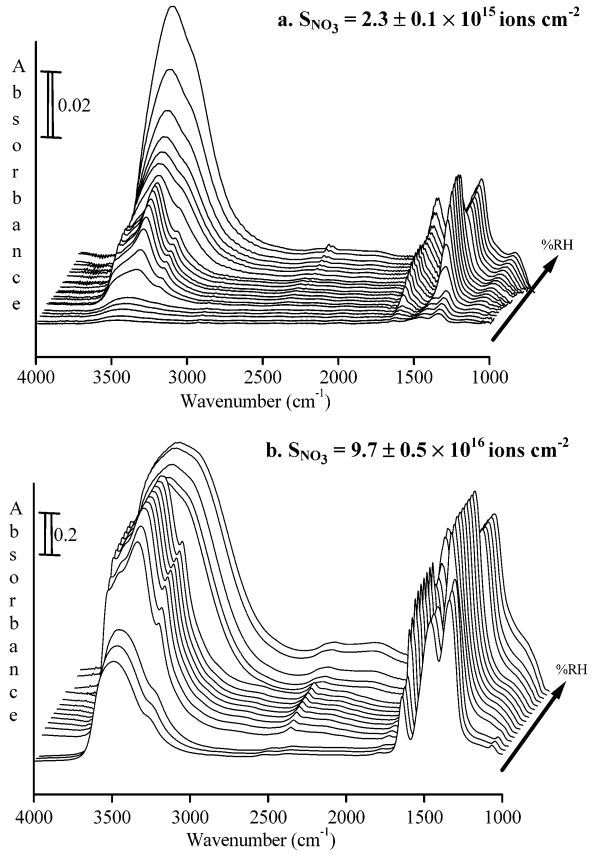

Figure 2. (a) Transmission FT-IR spectra of water adsorption on MgO(100) reacted previously with HNO_3 under dry conditions at a nitrate coverage of $(2.3 \pm 0.1) \times 10^{15}$ ions cm^{-2}. The spectra are recorded as a function of increasing % RH; 0.57, 1.4, 2.3, 3.5, 4.4, 9.2, 14, 19, 24, 28, 33, 38, 43, 47, 52, 57, 62, 66, 76, 84, and 93. (b) Transmission FT-IR spectra of water adsorption on MgO(100) reacted previously with HNO_3 under wet conditions at a nitrate coverage of $(9.7 \pm 0.5) \times 10^{16}$ ions cm^{-2}. The spectra are recorded as a function of increasing % RH; 0.36, 0.60, 1.0, 2.4, 3.4, 18, 23, 27, 32, 36, 41, 46, 51, 62, 66, 76, 90, and 93.

2. Water Adsorption and Desorption on Nitric Acid Reacted MgO(100). Water adsorption and desorption isotherms on nitrated MgO(100) surfaces following reaction with nitric acid were measured at 296 K. Transmission FT-IR spectra of water adsorption on MgO(100) reacted previously with nitric acid at two different nitrate film coverages are shown in Figure 2. Besides observing an overall increase in intensity in the absorption bands associated with the bending mode, $\delta(H_2O)$, and the O−H stretching mode, υ(OH), of adsorbed water in the spectral regions extending from 1500 to 1800 and 2800 to 3800 cm^{-1}, respectively, the spectra show very interesting

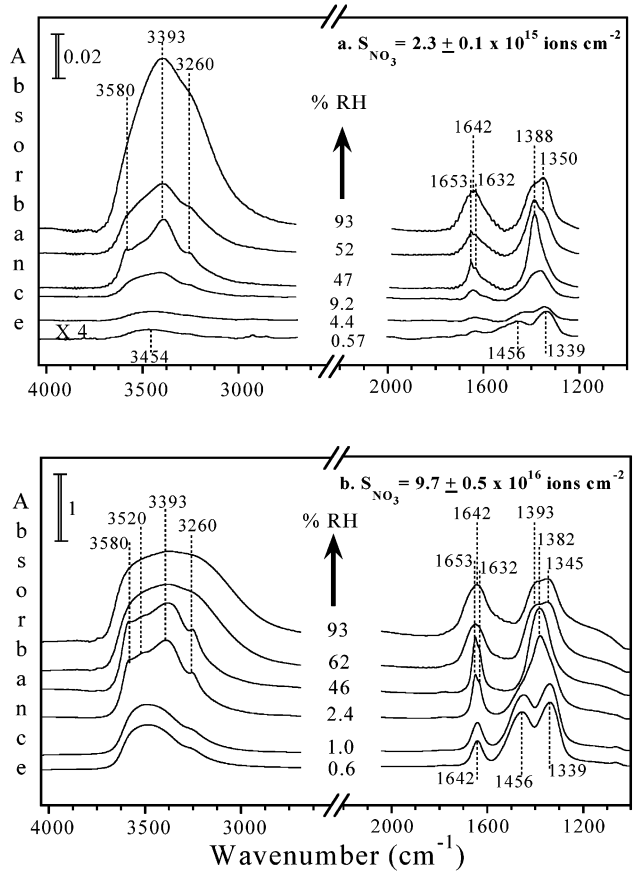

Figure 3. (a) Selected FT-IR spectra in the spectral range from 1000 to 2000 and 3000 to 4000 cm^{-1} following water adsorption on MgO(100) reacted with nitric acid at a coverage of $(2.3 \pm 0.1) \times 10^{15}$ ions cm^{-2}. Spectra show changes in the nitrate ion and water regions in three distinct regimes: (from bottom to top); <7% RH, 7−50% RH, and >50% RH. (b) Selected FT-IR spectra in the spectral range from 1000 to 2000 and 3000 to 4000 cm^{-1} following water adsorption on MgO(100) reacted with nitric acid at a coverage of $(9.7 \pm 0.5) \times 10^{16}$ ions cm^{-2}. Spectra show changes in the nitrate ion and water regions in three distinct regimes: (from bottom to top); <2% RH, 2−55% RH, and >55% RH.

changes in the nitrate spectral features as a function of increasing water vapor pressure as well.

The spectral changes observed in the nitrate and water absorption bands correspond to three distinct relative humidity ranges, which are, approximately, less than 10% RH, between ∼10 and 50% RH, and greater than ∼50% RH. Enlarged views of the observed spectral changes in the water and nitrate absorption bands for these three relative humidity ranges are shown in several representative spectra plotted in Figure 3. For the nitrate ion at the lowest RH, the $\upsilon_3(NO_3^-)$ band is seen as a doublet at 1339 and 1456 cm^{-1}. As the RH increases this doublet changes to a singleton centered at 1388 and 1382 cm^{-1} for nitrate coverages of $(2.3 \pm 0.1) \times 10^{15}$ and $(9.7 \pm 0.5) \times 10^{16}$ ions cm^{-2}, respectively. The singleton then appears to broaden and develop into two overlapping absorptions at the highest RH. Simultaneously, the absorption band of the bending mode of water is weak and symmetrically centered around 1642 cm^{-1}, beginning to narrow and grow in intensity as it shifts toward 1653 cm^{-1}. This band also shows a distinct shoulder at 1632 cm^{-1} between 14 and 47% RH and between 2.4 and 51% RH for nitrate coverages of $(2.3 \pm 0.1) \times 10^{15}$ and $(9.7 \pm 0.5) \times 10^{16}$ ions cm^{-2}, respectively. The shoulder on the water bending mode absorption is also observed in all spectra recorded as a function of decreasing RH but in different RH ranges. The

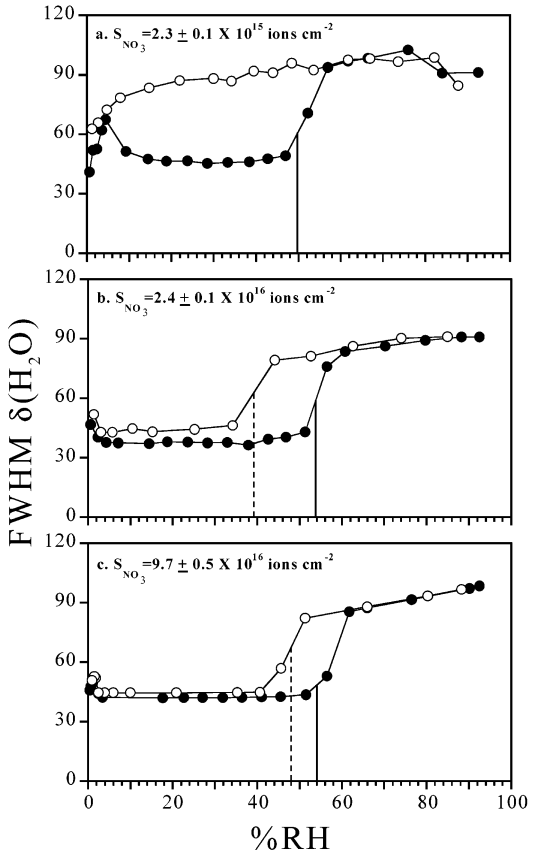

Figure 4. Full-width-at-half-maximum (fwhm) of the water bending mode plotted as a function of % RH for water adsorption/desorption on reacted MgO(100) surface as a function of nitrate film thickness: (a) $S_{NO_3} = (2.3 \pm 0.1) \times 10^{15}$ ions cm^{-2}; (b) $S_{NO_3} = (2.4 \pm 0.1) \times 10^{16}$ ions cm^{-2}; (c) $S_{NO_3} = (9.7 \pm 0.5) \times 10^{16}$ ions cm^{-2}. Phase transitions for deliquescence and efflorescence are marked by solid and dashed lines, respectively. See text for further details.

presence of this shoulder in the bending mode of water suggests that water molecules are in two different coordination environments owing to the high polarization power of the Mg^{2+} cation.[14] Above 50% RH, the bending mode absorption band broadens by nearly 50 cm^{-1} and forms a well-resolved symmetric band centered at 1642 cm^{-1}, a value close to that of bulk liquid water.[18] The O−H stretching mode region also shows changes in the structure of the broad band as a function of RH. The FT-IR spectra following water desorption as a function of RH show similarly interesting changes in the water and nitrate spectral features but at different RH, as discussed in more detail in the following paragraphs.

Further analysis of the bending mode of adsorbed water clearly shows a large change in the full-width-at-half-maximum (fwhm) of the bending mode, $\delta(H_2O)$. The fwhm analysis of the bending mode within the RH ranges where a shoulder is present at 1632 cm^{-1} may introduce an error to the fwhm values obtained in those RH ranges. Nevertheless, those values have been compared to the fwhm of a standard reference as discussed below obtained in the same spectral range. Figure 4 shows the fwhm of the water bending mode plotted as a function of % RH for water adsorption and desorption on the nitric acid reacted MgO(100) surface as a function of nitrate film thickness: (a) $S_{NO_3} = (2.3 \pm 0.1) \times 10^{15}$, (b) $S_{NO_3} = (2.4 \pm 0.1) \times 10^{16}$, and (c) $S_{NO_3} = (9.7 \pm 0.5) \times 10^{16}$ ions cm^{-2}, respectively. The fwhm clearly gets larger at the higher relative humidities. These changes are consistent with a phase change to an aqueous phase at higher RH as in magnesium nitrate solutions where $\delta(H_2O)$

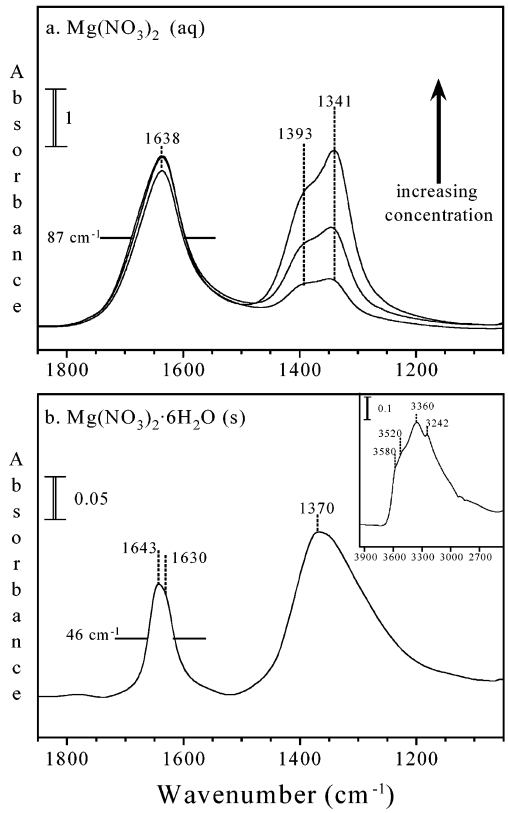

Figure 5. (a) ATR FT-IR spectra of magnesium nitrate solutions at 296 K as a function of concentration (0.29, 0.58, and 1.16 M). The spectral region extending from 1000 to 1900 cm^{-1} is shown. (b) ATR FT-IR spectrum of crystalline $Mg(NO_3)_2 \cdot 6H_2O$ at 296 K at 40% RH in the spectral region extending from 1000 to 1900 cm^{-1}. The OH stretch region extending from 3900 to 2600 cm^{-1} is shown in the inset. Absorbance spectra shown here were corrected for the variation of intensity as a function of wavelength.[19]

has a fwhm of 87 cm^{-1} (vide infra) close to the value of the fwhm seen in the spectra shown in Figure 4 at the higher relative humidities.

To interpret these changes in the FT-IR spectra as a function of RH, complementary ATR FT-IR spectra were collected of magnesium nitrate solutions and $Mg(NO_3)_2 \cdot 6H_2O$ crystals. The ATR FT-IR absorbance spectra reported here were corrected for the variation of intensity as a function of wavelength so as to compare to absorbance spectra obtained from transmission measurements.[19] Solution spectra are shown in Figure 5a. These spectra are similar to what has been observed previously for magnesium nitrate solutions.[20] The solution-phase spectra look very similar to the spectra taken at high relative humidity for the nitrated magnesium oxide surfaces shown in Figure 3. Figure 5b shows the nitrate asymmetric stretch and water bending mode region of $Mg(NO_3)_2 \cdot 6H_2O$ crystals held at 40 ± 1% RH at 296 K. The inset shows the O-H stretching mode region. The mid-IR spectrum of magnesium nitrate hexahydrate has been studied previously and the data from that study[14] and the ATR results from this study can be used to aid in the interpretation of the spectra shown in Figures 2 and 3. The literature spectrum[14] for the hexahydrate shows a single band for $\upsilon_3(NO_3^-)$ centered near 1364 cm^{-1}, in agreement with the spectrum shown in Figure 5b. There is also a well-defined doublet at 1636 and 1650 cm^{-1} for the water bending, $\delta(H_2O)$, with a fwhm of 46 cm^{-1}.[14] Before the phase change to the aqueous phase, the values of the fwhm are close to 45 cm^{-1} the same value for crystalline $Mg(NO_3)_2 \cdot 6H_2O$ reported in the literature[14] and measured here for a standard reference sample of $Mg(NO_3)_2 \cdot 6H_2O$ with ATR FT-IR spectroscopy. In addition, changes in the structure of the υ(OH) band suggests perturbation of the hydrogen bonding network as a function of RH. It is known that the presence of anions and cations affects the structure of liquid water.[21] The extent of structural perturbation will depend on the concentration of ions and the water coordination environment.

On the basis of the changes observed in the fwhm of the water bending mode and changes in the O−H stretching region of the spectra along with the standard spectra of crystalline magnesium nitrate hexahydrate and magnesium nitrate solutions, changes in the spectra shown in Figures 2 and 3 can be interpreted in terms of two phase transitions occurring as a function of RH. At low RH, it appears that the nitrate ion changes its coordination and phase from a metastable magnesium nitrate solid to a crystalline magnesium nitrate hydrate. Water also changes its environment from surface adsorbed water to water molecules incorporated in the lattice of the crystalline hydrate. At higher RH, the crystalline salt deliquesces to form a saturated solution layer on the surface. The deliquescence point occurs when the relative humidity above the solid reaches a value higher than that above the salt saturated solution at 298 K, which is 53 ± 2%.[22,23] For bulk samples, the molarity of the saturated solution of magnesium nitrate is 4.8 M at 298 K.[22]

To determine the exact RH for these phase transitions, two methods were employed. The first uses the fwhm of the bending mode of adsorbed water to determine the deliquescence, crystalline-phase to solution-phase transition, as a function of increasing RH, and efflorescence, solution-phase to crystalline-phase transition, as a function of decreasing RH. The transition points are marked in Figure 4 with solid (deliquescence) and dashed (efflorescence) lines midway between the two data points where there is a change in the fwhm of $\delta(H_2O)$. In the case of deliquescence, there is a sudden increase in the fwhm of $\delta(H_2O)$, and in the case of efflorescence, there is a sudden decrease in the fwhm of $\delta(H_2O)$. The second method employs the variance method described by Martin et al.[24] of consecutive IR spectra. Here the variance of the nitrate absorption band, $\upsilon(NO_3^-)$, is analyzed. The variance method is done by taking spectra collected at small increments (2−8%) of increasing RH, subtracting out gas-phase absorptions and then normalizing the absorbance of the nitrate absorption to one. Difference IR spectra are then calculated by subtracting each spectrum from the next higher % RH spectrum. The variance of the resultant difference spectrum is then calculated and normalized to the % RH step. The normalized-variance is then plotted as a function of the average % RH between consecutive steps. This analysis shown in Figure 6 for water adsorption/desorption spectra, i.e., increasing and decreasing % RH, on the reacted MgO(100) surface as a function of nitrate film thickness. Both the water adsorption and desorption data show two transitions for all nitrate films except for the thinnest film $<10^{16}$ nitrate ions cm^{-2}, for which there are no transitions observed upon decreasing RH. For the adsorption series, the position of the first transition is almost the same for the two thicker nitrate films $>10^{16}$ nitrate ions cm^{-2}, 2 ± 1%. The same transition occurs at 7% for the thinnest nitrate film, $(2.3 \pm 0.1) \times 10^{15}$ ions cm^{-2}. This transition is proposed to be from a metastable nitrate film and surface adsorbed water to a crystalline magnesium nitrate hydrate. The second transition is shown to occur at 49 ± 3% for the $(2.3 \pm 0.1) \times 10^{15}$ and at 54 ± 2% for the $(2.4 \pm 0.1) \times 10^{16}$ and the $(9.7 \pm 0.5) \times 10^{16}$ ions cm^{-2} nitrate film thickness. This second transition is proposed to be the deliquescence of the crystalline

TABLE 1: Phase Transitions in $Mg(NO_3)_2$ Thin Films Supported on MgO at 296 K

	% RH values corresponding to phase transitions in thin $Mg(NO_3)_2$ films				
	increasing %RH		decreasing %RH		
				efflorescence	
S_{NO_3} (ions cm^{-2})	metastable solid to crystalline hydrate	deliquescence	crystalline hydrate to metastable solid	% RH	S^*
$(2.3 \pm 0.1) \times 10^{15}$	7 ± 2	49 ± 2	[a]	[a]	
$(2.4 \pm 0.1) \times 10^{16}$					
first	2 ± 1	54 ± 2	2 ± 1	39 ± 5	3.4
second	4 ± 1	52 ± 2	3 ± 1	37 ± 6	2.8
$(9.7 \pm 0.5) \times 10^{16}$					
first	2 ± 1	54 ± 2	2 ± 1	48 ± 3	1.9
second	2 ± 1	56 ± 1	2 ± 1	45 ± 3	2.0

[a] Smooth transition from aqueous nitrate to metastable magnesium nitrate solid without formation of the crystalline hydrate phase.

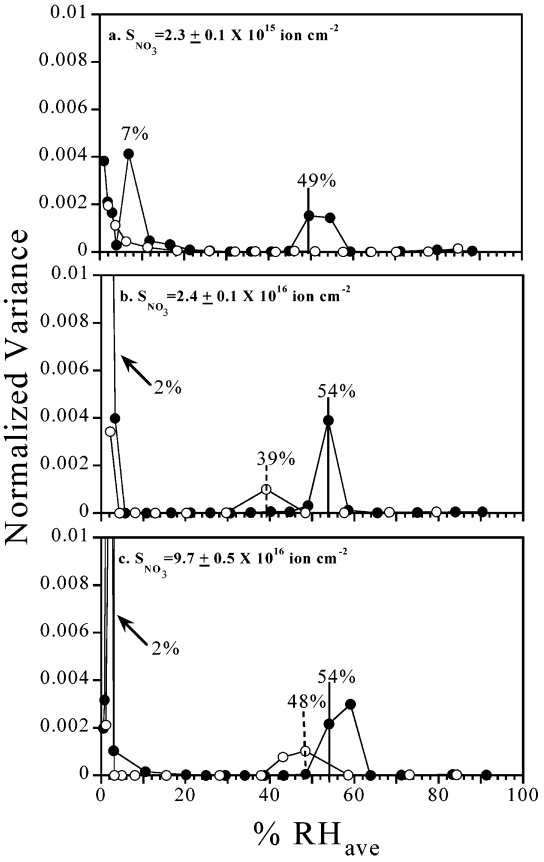

Figure 6. Normalized variance of the difference spectrum between two consecutive IR spectra in the nitrate absorption spectral region extending from 1215 to 1508 cm^{-1} plotted as a function of increasing RH and as a function of decreasing RH on nitric acid reacted MgO(100) surfaces of differing nitrate coverages: (a) $S_{NO_3} = (2.3 \pm 0.1) \times 10^{15}$ ions cm^{-2}; (b) $S_{NO_3} = (2.4 \pm 0.1) \times 10^{16}$ ions cm^{-2}; (c) $S_{NO_3} = (9.7 \pm 0.5) \times 10^{16}$ ions cm^{-2}. Phase transitions for deliquescence and efflorescence are marked by solid and dashed lines, respectively. See text for further details.

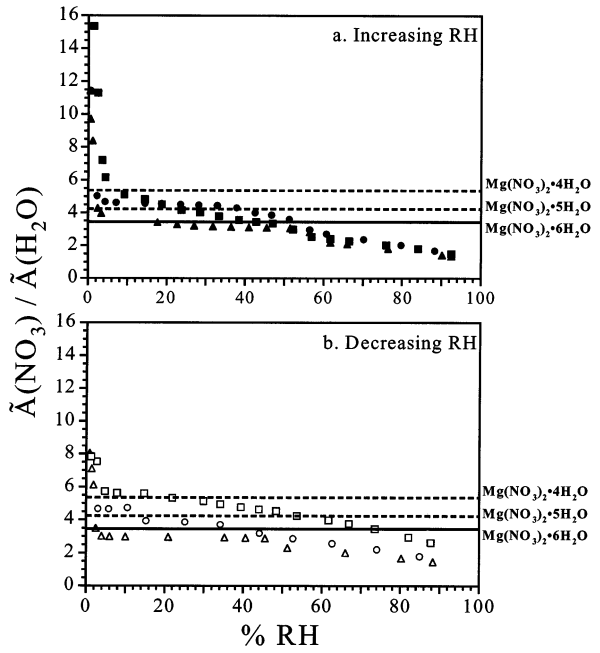

Figure 7. Ratio of the integrated absorbance of the $\upsilon_3(NO_3^-)$ to $\delta(H_2O)$ bands as a function of relative humidity. Data are shown for increasing (filled symbols) and decreasing (empty symbols) RH for the three nitrate coverages invesitigated: squares are for films with $S_{NO_3} = (2.3 \pm 0.1) \times 10^{15}$ ions cm^{-2}; circles are films with $S_{NO_3} = (2.4 \pm 0.1) \times 10^{16}$ ions cm^{-2}; triangles are for films with $S_{NO_3} = (9.7 \pm 0.5) \times 10^{16}$ ions cm^{-2}. The solid line represents the ratio of the integrated absorbance of the $\upsilon_3(NO_3^-)$ to $\delta(H_2O)$ bands obtained for a reference sample of $Mg(NO_3)_2 \cdot 6H_2O$ crystals. The dashed lines represent the ratio of the integrated absorbance predicted for $Mg(NO_3)_2 \cdot 5H_2O$ and $Mg(NO_3)_2 \cdot 4H_2O$ from stoichiometry and the ratio measured for the hexahydrate reference sample.

magnesium nitrate hexahydrate salt. A compilation of the % RH for the phase transitions observed in thin films of $Mg(NO_3)_2$ supported on magnesium oxide is given in Table 1. Two sets of data are given in Table 1 for the thicker films. One set of data corresponds to the first series of water adsorption/desorption experiments and the other to a second series of water adsorption/desorption measurements made on the same film.

The ratio of the integrated absorbance of the $\upsilon_3(NO_3^-)$ to $\delta(H_2O)$ bands and the spectral data shown in Figure 3 can provide some insight into the hydrate salt that forms on the surface after the low relative humidity phase transition and prior to deliquescence. Figure 7 shows the ratio of the integrated absorbance of the nitrate absorption band ($\upsilon_3(NO_3^-)$) to the water absorption band ($\delta(H_2O)$) as a function of relative humidity. Data are shown for increasing (filled symbols) and decreasing (empty symbols) RH for the three nitrate coverages invesitigated: $S_{NO_3} = (2.3 \pm 0.1) \times 10^{15}$, $(2.4 \pm 0.1) \times 10^{16}$, and $(9.7 \pm 0.5) \times 10^{16}$ ions cm^{-2}, respectively. The solid line represents the ratio of the integrated absorbance of the $\upsilon_3(NO_3^-)$ to $\delta(H_2O)$ bands obtained for the reference spectra of $Mg(NO_3)_2 \cdot 6H_2O$ crystals shown in Figure 5b. This ratio is 3.5 and is shown in Figure 7 as a solid line. The data shown in Figure 7 indicate that prior to deliquescence, the hydrate salt for all of the films has the stoichiometry of the magnesium nitrate hexahydrate. For films with nitrate coverages of $S_{NO_3} = (2.3 \pm 0.1) \times 10^{15}$ and $(2.4 \pm 0.1) \times 10^{16}$ ion cm^{-2}, the hydrate salt that forms immediately after crystallization has a ratio of $\upsilon_3(NO_3^-)$ to $\delta(H_2O)$ greater than 3.5 whereas for the thickest nitrate coverage, $(9.7 \pm 0.5) \times 10^{16}$ ions cm^{-2}, a ratio of $\upsilon_3(NO_3^-)$ to $\delta(H_2O)$ of

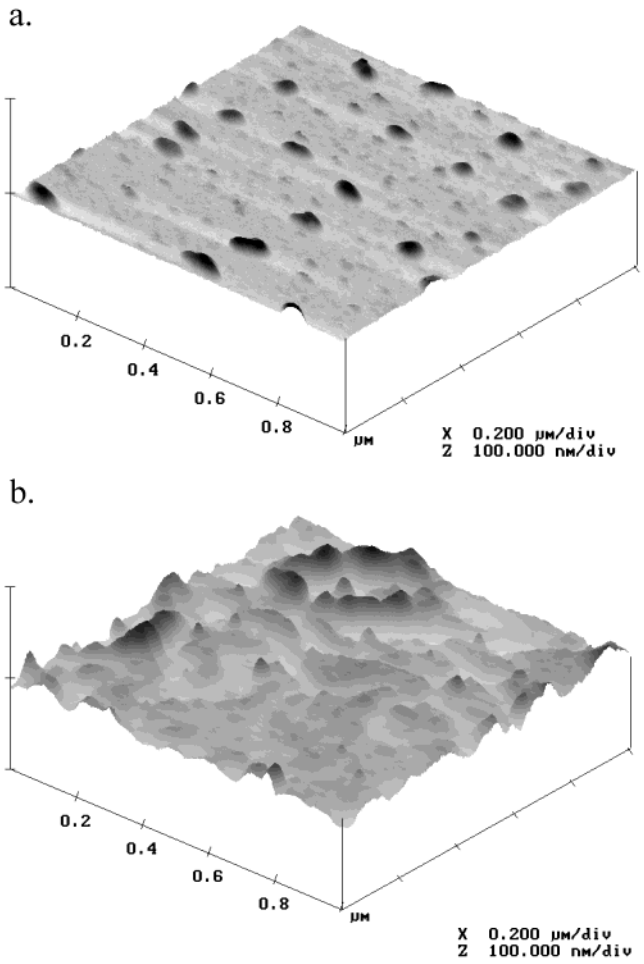

Figure 8. AFM images of the MgO(100) surface: (a) stored in a desiccator for several weeks before imaging; (b) reacted with nitric acid ($S_{NO_3} = (9.7 \pm 0.5) \times 10^{16}$ ions cm^{-2}) and subjected to several H_2O adsorption/desorption cycles.

very near 3.5 is observed upon crystallization. This observation suggests that immediately upon crystallization the hexahydrate forms for the thickest film whereas the thinner nitrate films form a different hydrate salt immediately after crystallization. Other stable hydrate forms of magnesium nitrate include $Mg(NO_3)_2 \cdot 4H_2O$ and $Mg(NO_3)_2 \cdot 5H_2O$. Using the ratio of the integrated absorbance of the $\upsilon_3(NO_3^-)$ to $\delta(H_2O)$ bands for the hexahydrate reference, the ratio of $\upsilon_3(NO_3^-)$ to $\delta(H_2O)$ predicted for $Mg(NO_3)_2 \cdot 4H_2O$ and $Mg(NO_3)_2 \cdot 5H_2O$ are 5.3 and 4.2, respectively, based on the stoichiometry of these hydrates. The dotted lines in Figure 7 represent the expected ratio for these two lower hydrates. Thus it can be seen from Figure 7a that for nitrate coverages $S_{NO_3} = (2.3 \pm 0.1) \times 10^{15}$ and $(2.4 \pm 0.1) \times 10^{16}$, a lower hydrate salt forms immediately upon crystallization as the RH increases. At 10% RH, it appears that the pentahydrate is formed for these two films and then there is a continuous uptake of water as the RH increases until the thermodynamically more stable hexahydrate salt forms and it is this hydrate that undergoes deliquescence around 50% RH. It is interesting to note that once deliquescence occurs and the solution layer forms, the ratio of the integrated absorbance of the $\upsilon_3(NO_3^-)$ to $\delta(H_2O)$ bands are the same for all three films. For the two films that undergo efflorescence, $S_{NO_3} = (2.4 \pm 0.1) \times 10^{16}$ and $(9.7 \pm 0.5) \times 10^{16}$ ions cm^{-2}, the data in Figure 7b show that the hexahydrate salt is nucleated after reaching 39 and 48% RH, respectively.

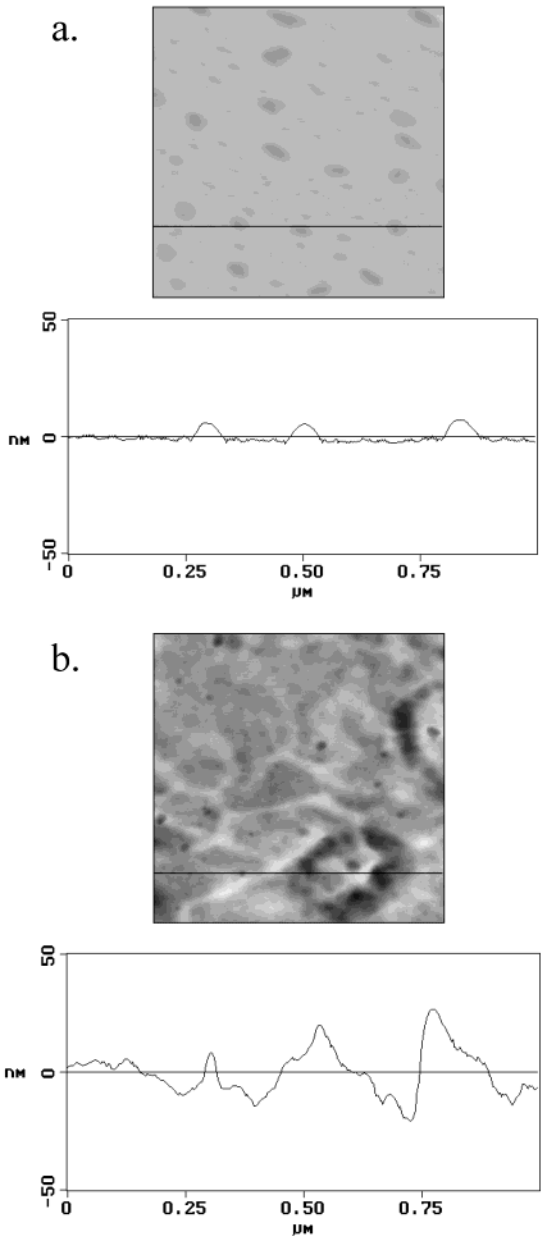

Figure 9. AFM cross section analysis of MgO(100) surfaces: (a) stored in a desiccator for several weeks before imaging; (b) reacted with HNO_3 ($S_{NO_3} = (9.7 \pm 0.5) \times 10^{16}$ ions cm^{-2}) and subjected to several H_2O adsorption/desorption cycles.

Further evidence for the formation of lower hydrates of magnesium nitrate is also evident upon careful examination of the IR spectra shown in Figure 3. In the spectra recorded immediately after the first phase transition, i.e., crystallization upon increasing RH, there is a nitrate band broader than that observed prior to crystallization. Specifically, there are changes observed in the spectrum taken at 9.2% RH for the thinnest film with a nitrate coverage of $S_{NO_3} = (2.3 \pm 0.1) \times 10^{15}$ ions cm^{-2} (Figure 3a) and the spectrum recorded at 47% RH. These changes are attributed to the conversion of $Mg(NO_3)_2 \cdot 5H_2O$ to $Mg(NO_3)_2 \cdot 6H_2O$ with increasing RH. The transition to the hexahydrate salt occurs smoothly as a function of increasing RH as water molecules replace nitrate ions in the first coordination sphere.

3. AFM Analysis of Nitric Acid Reacted MgO(100). The MgO(100) surface has been examined previously with atomic force microscopy.[25] AFM images of two different MgO(100)

surfaces are shown in both Figures 8 and 9. One surface was reacted with nitric acid and the other was not. The unreacted surface, Figure 8a, was calcined and stored in a desiccator for several weeks before imaging. The AFM image shows a nearly flat surface with hillocks present on top. Such features have been observed before for MgO surfaces cleaved and stored in an evacuated desiccator for several weeks before imaging. These features are assigned to $Mg(OH)_2$.[25] Figure 8b shows the AFM image for MgO(100) that has been reacted with nitric acid at 25% RH, $S_{NO_3} = (9.7 \pm 0.5) \times 10^{16}$ ions cm^{-2} and subjected to several H_2O adsorption/desorption cycles. The image clearly shows an increase in surface roughness for the nitric acid reacted surface. The images root-mean-square average height deviations from the mean plane (RMS) values show a factor of 4 increase in the roughness for reacted surface versus the unreacted one. Section analyses for the two surfaces shown in Figure 8 are given in Figure 9. Section analysis for the unreacted surface shows that the height of the hillocks is around 5 nm whereas that for the rough areas on the reacted surface ranges from 15 to 30 nm. Such changes in surface morphology upon reaction with nitric acid are consistent with the FT-IR results in that subsurface layers of the oxide are reacting with nitric acid and causing significant roughening of the surface.

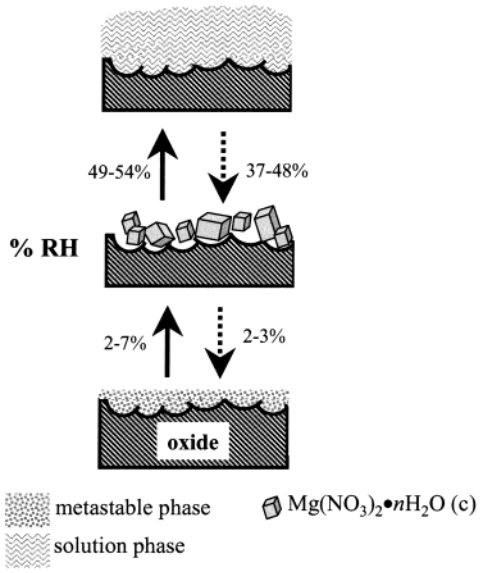

Figure 10. Schematic diagram showing phase transitions of nitrate films on MgO(100) surfaces as a function of relative humidity at 296 K observed in this study. The solid and dashed arrows are for increasing % RH and decreasing % RH, respectively. See text for further details.

Discussion

1. Mechanisms for Nitric Acid Adsorption under Dry and Wet Conditions. The ratio of the nitrate coverage to the MgO ion pair determined for nitric acid adsorption under dry conditions is approximately 2. This number is consistent with reactivity of the topmost layer only, according to reaction 2. In the presence of water vapor corresponding to 25% RH, nitrate coverages greater than 10 times the MgO ion pair surface density are obtained, indicating subsurface layers of the oxide surface are reacting with nitric acid. At 25% RH it is estimated that the water coverage on unreacted MgO(100) is on the order of two monolayers.[7] The fact that subsurface layers are reacting suggests that there is enough water to enhance ionic mobility on the surface similar to that established for NaCl surfaces. Laux et al.[26] and Allen et al.[27] found in their studies on NaCl(100) single crystals that a nitrate-saturated surface from reaction with HNO_3 undergoes reorganization upon water introduction to form microcrystallites of $NaNO_3$ induced by the enhancement of ion mobility in the presence of adsorbed water. In an elegant set of experiments using atomic force microscopy, Zangmeister and Pemberton[28] showed that prior to the formation of microcrystallites, mobile $NaNO_3$ strings formed on the surface. It is important to note that these mobile strings occur at a RH below that of the deliquescence RH of either NaCl or $NaNO_3$. We hypothesize that a similar mechanism may be operative here for the uptake of nitric acid on MgO at 25% RH. That is to say there is enough ionic mobility of $Mg(NO_3)_2$ to form microcrystallites of solid $Mg(NO_3)_2 \cdot nH_2O$ ($4 < n \leq 6$) on the host oxide crystal at RH values below the deliquescence point of $Mg(NO_3)_2 \cdot 6H_2O$. The phase transition data indicate that ionic mobility is quite facile around 2% RH for the thicker nitrate films and near 7% for the thinnest nitrate film studied. Ionic mobility enhances the reconstruction of the metastable nitrate film formed on MgO surfaces to the stable crystalline hydrate forms of $Mg(NO_3)_2$ upon water exposure.

2. Phase Transitions in Magnesium Nitrate Nanometer Thin Films Supported on MgO. From thermodynamic considerations, the relative stability of bulk magnesium hexahydrate and the anhydrous salt can be estimated using the appropriate values of standard ΔG_f [23] at 298 K for the following equilibrium:[29]

$$Mg(NO_3)_2(s) + 6H_2O(g) \rightleftharpoons Mg(NO_3)_2 \cdot 6H_2O(s) \quad (3)$$

An equilibrium water vapor pressure of 0.243 Torr is obtained, corresponding to 1.1% RH. At this RH, bulk anhydrous magnesium nitrate will transform to the hexahydrate.

In this study, changes that occur in thin magnesium nitrate films have been monitored during increasing and decreasing % RH. Several phase transitions have been identified. These transitions are depicted in the schematic cartoon shown in Figure 10. The transition that occurs at RH <10% has been proposed to be the conversion of metastable nitrate film to crystalline magnesium nitrate hydrate, $Mg(NO_3)_2 \cdot nH_2O$. For nitrate coverages $>10^{16}$ ions cm^{-2}, this transition occurs at a value close to that seen for reaction 3 in bulk samples. For the thinnest nitrate film, the transition is observed at 7% RH, indicating that for the thinnest nitrate film, the transition may be kinetically controlled. Immediately after crystallization, the number of water molecules, n, in $Mg(NO_3)_2 \cdot nH_2O$ depends on the thickness of the nitrate film. For nitrate coverages below $(9.7 \pm 0.5) \times 10^{16}$ ions cm^{-2}, evidence for the formation of the pentahydrate is suggested from the IR data. The pentahydrate salt continues to take up water and undergoes a smooth transition to the thermodynamically more stable magnesium nitrate hexahydrate, $Mg(NO_3)_2 \cdot 6H_2O$ phase prior to deliquescence.

As a function of increasing relative humidity, deliquescence of the hexahydrate salt, reaction 4, is observed. For the thicker nitrate films, the deliquescence relative humidity (DRH) at $54 \pm 2\%$ is within experimental error found for bulk solutions.

$$Mg(NO_3)_2 \cdot 6H_2O(s) \rightleftharpoons Mg^{2+}(aq) + 2NO_3^-(aq) \quad (4)$$

For the thinnest nitrate film, the DRH differs some from the thicker films and is observed at $49 \pm 2\%$. Although the DRH shows some dependence on film thickness, the efflorescence relative humidity (ERH) has an even greater dependence on film thickness as discussed below.

Efflorescence is defined as the homogeneous crystallization from solution.[30] It occurs when the supersaturation of a solution reaches a critical value necessary to induce nucleation.[31] Hysteresis effects when aqueous salt particles are being dried are well-known, and the difference between the deliquescence and efflorescence RH values is attributed to the slowness of critical germ formation upon drying.[32] In general, it is found that the presence of a germ or a nucleus in the saturated solution enhances crystallization at higher RH values relative to that for homogeneous efflorescence.[32]

In this study, reducing the vapor pressure of water will result in water evaporation from the surface up to the point where crystallization occurs. The ERH is observed at 39 ± 5% for the $S_{NO_3} = (2.4 \pm 0.1) \times 10^{16}$ ions cm^{-2} film and at 48 ± 3% for the $S_{NO_3} = (9.7 \pm 0.5) \times 10^{16}$ ions cm^{-2} film. Efflorescence was *not* observed for the thinnest nitrate film with a nitrate coverage of $(2.3 \pm 0.1) \times 10^{15}$ ion cm^{-2}. There are no data available for the homogeneous ERH of $Mg(NO_3)_2$. Other nitrate salts such as $NaNO_3$ and NH_4NO_3 systems show no homogeneous crystallization from aqueous solution even at low RH.[32] For nitrate film thickness $>10^{16}$ ions cm^{-2}, the ERH shifts to a higher value for the thickest film. These differences may be related to the density of nucleation sites on the nearly flat single-crystal surfaces of MgO(100) upon reaction with HNO_3. The thinner nitrate film undergoes deliquescence but not efflorescence, most likely because of the large energy barrier associated with crystallization in the absence of nucleation sites. In a study by Lightstone et al.,[31] the effect of inclusion of solid succinic acid on the deliquescence and efflorescence behavior of ammonium nitrate/water microdroplets was examined. Increasing the diameter of the succinic acid inclusions increased the efflorescence rate and thus decreased the supersaturation necessary for efflorescence. The increase in the number of potential nucleation sites is proportional to the increase in surface area as a result of increasing the diameter of succinic acid inclusions. Nucleation sites on the succinic acid surface catalyze the formation of the critical embryo by decreasing the nucleation barrier height. For the NH_4NO_3/succinic acid system, it was found that the number of molecules in the critical embryo calculated using the classical nucleation theory increases as the diameter of succinic acid inclusions increases. A similar type of analysis for the efflorescence of magnesium nitrate hexahydrate measured in this study is presented here. The relative number of sites in the critical embryo can be determined from the efflorescence data of the two thicker films. The critical supersaturation, S^*, of aqueous magnesium nitrate with respect to the crystalline magnesium nitrate hexahydrate can be calculated using[31,33]

$$\ln S^* = -\int_{\mathrm{DRH}}^{\mathrm{ERH}} \frac{x_{H_2O}}{x_{NO_3}} \, \mathrm{d} \ln \mathrm{RH} \tag{5}$$

where x_{H_2O}/x_{NO_3} is the mole ratio of water to nitrate in the solution phase. The value of S^* can be determined from the area under the curve of x_{H_2O}/x_{NO_3} calculated from the surface density of water molecules for each nitrate film as a function of decreasing RH versus $-\ln$ RH. The calculated values of S^* are listed in Table 1 for each nitrate film. The relationship between S^* and the number of molecules in the critical embryo, g^*, is

$$\frac{W^*}{kT} = \frac{1}{2} g^* \ln S^* \tag{6}$$

where W^* is the nucleation barrier and is a function of the surface tension between the solid and the solution, the molecular volume in the solid, the contact angle between the critical nucleus of the solid and the surface, the temperature, and the critical supersaturation, k is Boltzman constant, and T is the temperature. The ratio of the number of molecules in the critical embryo formed for one nitrate film relative to another will lead to the cancellation of most of the terms with the assumption that the contact angle is the same for the nuclei formed on both films. Therefore, the resulting expression will be a relationship between g^* and S^*, as shown in eq 7:

$$\frac{g_1^*}{g_2^*} \approx \left(\frac{\ln S_2^*}{\ln S_1^*} \right)^3 \tag{7}$$

For the efflorescence observed for the $S_{NO_3} = (2.4 \pm 0.1) \times 10^{16}$ ions cm^{-2} and $S_{NO_3} = (9.7 \pm 0.5) \times 10^{16}$ ions cm^{-2} films, the ratio of the natural log of the critical supersaturation value indicates that the number of molecules formed in the critical embryo on the thickest film is about 3−7 times greater than that on the thinner film and at least 20 times greater than that of the thinnest film. These values can be taken as estimates for the increase in the number of nucleation sites observed for thick nitrate films formed on the expense of the host MgO surface.

The efficiency of heterogeneous nucleation of ammonium sulfate from supersaturated solutions due to the presence of mineral oxide particles has been discussed by Martin et al.[34] It was found that the efficiency of germ formation for different oxide particles could be correlated to the crystallographic surface structure of the mineral oxide on which the germ grows. Figure

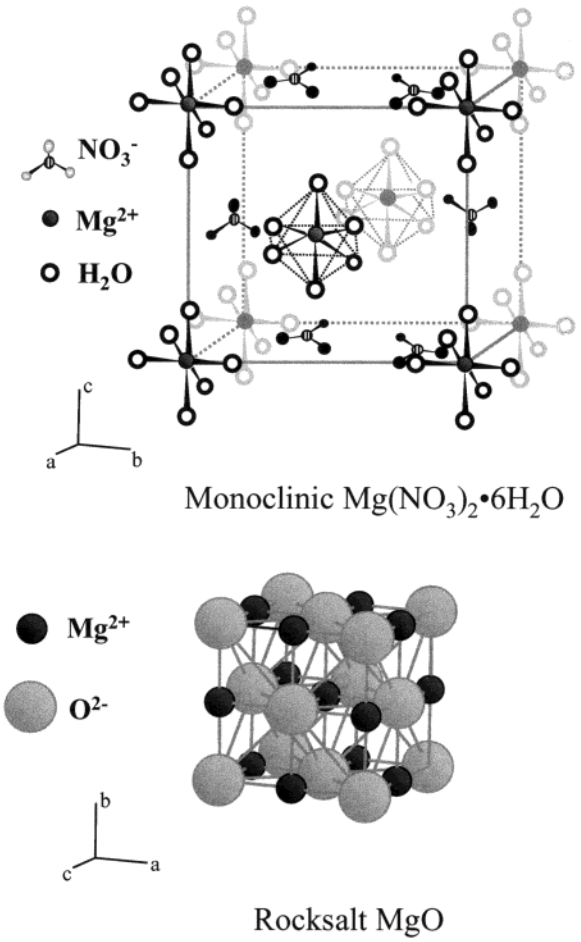

Figure 11. Bulk crystal structure of monoclinic $Mg(NO_3)_2 \cdot 6H_2O$ (a = 6.19, b = 12.7, and c = 6.6 Å) and rock salt MgO (a = 4.2 Å).

11 shows the bulk crystal structure of both $Mg(NO_3)_2 \cdot 6H_2O$ and MgO. The crystal structure of $Mg(NO_3)_2 \cdot 6H_2O$ is monoclinic with cell parameters $a = 6.19$, $b = 12.7$, and $c = 6.6$ Å[35] whereas the structure of MgO is rock salt with a cell parameter of 4.2 Å[3]. In this study here, it is observed that MgO(100) does not nucleate $Mg(NO_3)_2 \cdot 6H_2O$ for thin films but does so for thicker films despite having a different crystalline structure. Thus, we conclude that the efflorescence of $Mg(NO_3)_2 \cdot 6H_2O$ is controlled by the density of defects and therefore the density of nucleation sites on the oxide crystal. Thicker nitrate films form from reaction of subsurface layers of MgO. This process increases the roughness of the flat single-crystal surface, as seen in the AFM images shown in Figures 8 and 9. An increase in the surface roughness will result in an increase in the density of nucleation sites, which acts to lower the nucleation barrier and leads to an ERH within ~6% of the DRH for the thicker films.

3. Quantifying Nitrate and Water Coverages. The adsorbed nitrate and water coverages were calculated using eq 1 given in the Results. In this section, approximations made in the calculations and the greatest uncertainty in these calculations are discussed.

Nitrate coverages were calculated using a value of the integrated cross section, $\bar{\sigma}$, for the nitrate absorption in the spectral range extending from 1200 to 1500 cm^{-1} determined for nitrate ion using ATR FT-IR spectra recorded for $Mg(NO_3)_2$ solutions. In these calculations the nitrate integrated cross section is determined relative to the known integrated cross section for the bending mode of liquid water. In the spectral range extending from 1520 to 1770 cm^{-1}, $\bar{\sigma}$ is 5.73×10^{-18} cm $molecule^{-1}$ for liquid water at 298 K.[36] From several measurements of $Mg(NO_3)_2$ at concentrations near 1 M, a value of $\bar{\sigma} = (2.4 \pm 0.1) \times 10^{-16}$ cm ion^{-1}, is determined. This calculation is similar to that done by Sporleder and Ewing in their work on sodium nitrate solutions.[17] The value of $\bar{\sigma} = (2.4 \pm 0.1) \times 10^{-16}$ cm ion^{-1} is within 30% of that calculated for nitrate in $NaNO_3$ solutions and $NaNO_3$ solid. The nitrate ion coverage was determined only from the spectra recorded at a RH above the deliquescence of the film when the nitrate ion was in an aqueous environment similar to that of the standard ATR spectra used to calculate $\bar{\sigma}$. From the approximations used in these calculations, the absolute nitrate coverage may be as much as a factor of 2 different from that reported here.

Adsorbed water coverages were determined using the integrated absorbance of the bending mode, $\delta(H_2O)$. The bending mode of adsorbed water is sensitive to the water environment and the strength of hydrogen bonding.[37] As discussed by Irish and Chang,[20] polarization of water by the Mg^{2+} ion in $Mg(NO_3)_2$ solutions increases the molar intensity of the bending mode and shifts it to higher frequency. Therefore, the integrated cross section of the bending mode of water will be higher in the $Mg(NO_3)_2 \cdot 6H_2O$ system than in liquid water. The integrated cross section of $\delta(H_2O)$ in this study has been approximated from the fact that the first spectrum recorded after deliquescence corresponds to a saturated solution of $Mg(NO_3)_2$ with a water to a nitrate molar ratio of 3:1. Thus, water coverage in molecules cm^{-2} at the deliquescence point can be obtained from the nitrate coverage calculated at that point. The integrated absorbance of $\delta(H_2O)$ in the spectra recorded after deliqusence and eq 1 can be used to calculate $\bar{\sigma}$ of $\delta(H_2O)$, which is found to be equal to $(2.77 \pm 0.3) \times 10^{-17}$ cm $molecule^{-1}$. Figure 12 shows a plot of the water uptake on nitric acid reacted at MgO(100) for different nitrate coverages, (a) $(2.3 \pm 0.1) \times 10^{15}$, (b) $(2.4 \pm 0.1) \times 10^{16}$, and (c) $(9.7 \pm 0.5) \times 10^{16}$ ions cm^{-2}, as a function

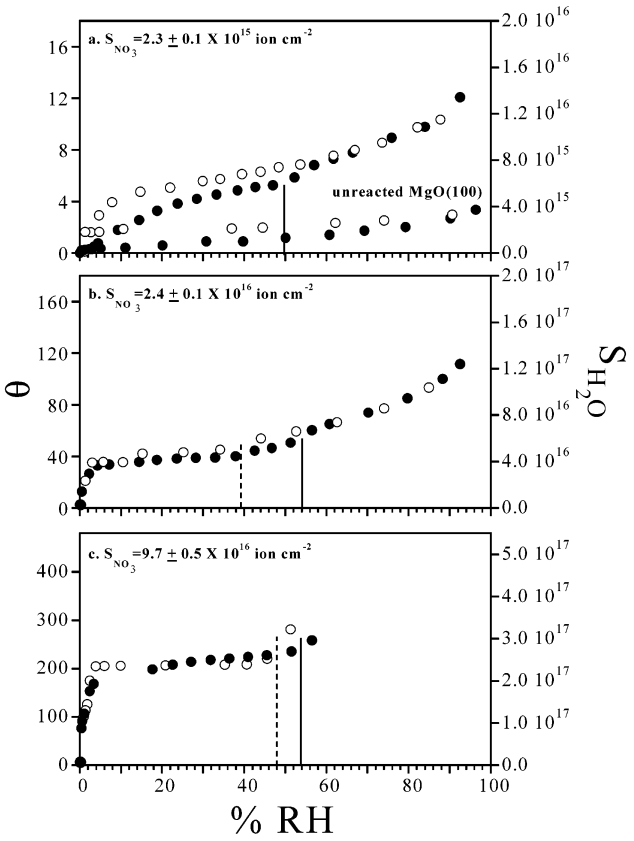

Figure 12. Water adsorption isotherms at $T = 296$ K as a function of relative humidity on nitric acid reacted MgO(100) (increasing RH, filled circles; decreasing RH, open circles). The water coverages were calculated using the bending mode and eq 1. See text for further details. Phase transitions for deliquescence and efflorescence are marked by solid and dashed lines, respectively, for films of different nitrate coverages: (a) $S_{NO_3} = (2.3 \pm 0.1) \times 10^{15}$ ions cm^{-2}; (b) $S_{NO_3} = (2.4 \pm 0.1) \times 10^{16}$ ions cm^{-2}; (c) $S_{NO_3} = (9.7 \pm 0.5) \times 10^{16}$ ions cm^{-2}. The water adsorption/desorption isotherm on unreacted MgO(100) is also shown in (a), note that there is significantly less water taken up by the unreacted surface.

of relative humidity (increasing RH, filled circles; decreasing RH, open circles). For the thickest films, the region above 60% RH is not shown. This is because the films were so thick that the absorbance of the liquid film was beyond the linear range of Beer−Lambert's law. The approximation made in calculating the water coverage is that the integrated cross section for the bending mode is constant as a function of relative humidity.

The data shown in Figure 12 are plotted in terms of S_{H_2O} in units of molecules cm^{-2} and monolayers, θ. For surface coverage in monolayers, the amount of adsorbed water has been normalized to the MgO(100) ion pair density, 1.13×10^{15} ions cm^{-2}. Water uptake on the unreacted MgO(100) is also shown in Figure 12a and is in agreement with published water adsorption isotherms on MgO(100).[7] The data show that the water adsorption properties of the MgO(100) surface after reaction with nitric acid are significantly altered.

Conclusions

The heterogeneous reaction of nitric acid with MgO(100) under dry and wet conditions has been investigated using FT-IR spectroscopy. The presence of gas-phase water enhances the uptake of nitric acid on the surface and results in further reaction of subsurface layers. The enhanced reactivity is most likely due to an increase in the ionic mobility of Mg^{2+} and NO_3^- in the presence of adsorbed water whereby magnesium nitrate can form

crystallites on the host oxide exposing additional sites for further reaction. Water adsorption experiments on the reacted MgO surface as a function of increasing relative humidity reveal two phase transitions. These transitions correspond to the conversion of a metastable amorphous phase of magnesium nitrate and surface adsorbed water to a crystalline hydrate salt, $Mg(NO_3)_2 \cdot nH_2O$ ($4 < n \leq 6$). The hexahydrate salt forms for all films as the RH increases. The deliquescence of the hexahydate salt occurs at 49 ± 2% RH for thin films and 54 ± 2% RH for thicker films. A hysteresis is seen as a function of decreasing relative humidity, and the transition corresponding to efflorescence depends to an even greater extent on film thickness. Efflorescence is not observed for the thinnest magnesium nitrate films studied. This study shows that phase transitions in thin films, tens to hundreds of nanometers thick, have very different behaviors than found in the bulk phase. Information gleaned from the experiments reported here may be insightful in understanding surface reactions and surface properties of interfaces present at ambient conditions.

Acknowledgment. We thank Charles Schutte for providing the ATR FT-IR data for magnesium nitrate solutions and Jean Ross and Randy Nessler for their help in collecting AFM images at the Central Microscopy Research Facility. We gratefully acknowledge the National Science Foundation for support of this work (CHE-9988434).

References and Notes

(1) Blesa, M.; Morando, P.; Regazzoni, A. *Chemical Dissolution of Metal Oxides*; CRC Press: Boca Raton, FL, 1993.

(2) Stumm, W. *Chemistry of the Solid-Water Interface: Processes at the Mineral-Water and Particles-Water Interface in Natural Systmes*; John Wiley and Sons: NewYork, 1978.

(3) West, A. R. *Basic Solid State Chemistry*, 2nd ed.; John Wiley & Sons Ltd.: New York, 2000.

(4) Stefanovich, E. V.; Truong, T. N. *J. Chem. Phys.* **1995**, *102*, 5071.

(5) Giordano, L.; Goniakowski, J.; Suzanne, J. *Phys Rev. Lett.* **1998**, *18*, 1271.

(6) Lyden-Bell, R. M.; Site, L. D.; Alavi, A. *Surf. Sci.* **2002**, *496*, L1.

(7) Foster, M.; Furse, M.; Passno, D. *Surf. Sci.* **2002**, *502*−*503*, 102.

(8) Johnson, M. A.; Stefanovich, E. V.; Truong, T. N.; Günster, J.; Goodman, D. W. *J. Phys. Chem. B* **1999**, *103*, 3391.

(9) Günster, J.; Liu, G.; Stultz, J.; Krischok, S.; Goodman, D. W. *J. Phys. Chem. B* **2000**, *104*, 5738.

(10) Kim, H. D.; Lynden-Bell, R. M.; Alavi, A.; Stultz, J.; Goodman, D. W. *Chem. Phys Lett.* **2002**, *352*, 318.

(11) Kim, J.; Schmitt, U.; Gruetzmacher, J.; Voth, G.; Scherer, N. *J. Chem. Phys.* **2002**, *116*−*2*, 737.

(12) Al-Abadleh, H. A.; Grassian, V. H. *Langmiur* **2003**, *19*, 341.

(13) Cantrell, W.; Ewing, G. E. *J. Phys. Chem. B* **2001**, *105*, 5434.

(14) Chang, T. G.; Irish, D. E. *Can. J. Chem.* **1973**, *51*, 118.

(15) Addison, C. C.; Walker, A. *J. Chem. Soc., London* **1963**, *Pt. 1*, 1220.

(16) Hemminger, J. C. *Int. Rev. Phys. Chem.* **1999**, *18*, 387.

(17) Sporleder, D.; Ewing, G. E. *J. Phys. Chem. A* **2001**, *105*, 1838.

(18) Eisenberg, D.; Kauzmann, W. *The Structure and Properties of Water*; Oxford University Press: New York, 1969.

(19) Hind, A. R.; Bhargava, S. K.; McKinnon, A. *Adv. Colloid Interface Sci.* **2001**, *93*, 91.

(20) Chang, T. G.; Irish, D. E. *J. Phys. Chem.* **1973**, *77*, 52.

(21) Franks, F. *Water: A comprehensive treatise*; Plenum Press: New York, 1973; Vol. 3.

(22) Apelblat, A. *J. Chem. Thermodyn.* **1992**, *24*, 619.

(23) *CRC Handbook of Chemistry and Physics*, 72nd ed.; CRC Press: Boca Raton, FL, 1991.

(24) Martin, S. T.; Han, J.-H.; Hung, H.-M. *Geophys. Res. Lett.* **2001**, *28*, 2601.

(25) Liu, P.; Kendelewicz, T.; Brown Jr., G. E.; Parks, G. A. *Surf. Sci.* **1998**, *412*/*413*, 287.

(26) Laux, J. M.; Fister, T. F.; Finlayson-Pitts, B. J.; Hemminger, J. C. *J. Phys. Chem.* **1996**, *100*, 19891.

(27) Allen, H. C.; Laux, J. M.; Vogt, R.; Finlayson-Pitts, B. J.; Hemminger, J. C. *J. Phys. Chem.* **1996**, *100*, 6371.

(28) Zangmeister, C. D.; Pemberton, J. E. *J. Phys. Chem. B* **1998**, *102*, 8950.

(29) Tang, I. N.; Fung, K. H. *J. Chem. Phys.* **1997**, *106*, 1653.

(30) Cantrell, W.; Charles, M.; Ewing, G. E. *J. Chem. Phys.* **2002**, *116*, 2116.

(31) Lightstone, J. M.; Onasch, T. B.; Imre, D.; Oatis, S. *J. Phys. Chem. A* **2000**, *104*, 9337.

(32) Martin, S. T. *Chem. Rev.* **2000**, *100*, 3403.

(33) Richardson, C. B.; Snyder, T. D. *Langmiur* **1994**, *10*, 2462.

(34) Martin, S. T.; Schlenker, J.; Chelf, J. H.; Duckworth, O. W. *Environ. Sci. Technol.* **2001**, *35*, 1624.

(35) Braibanti, A.; Triripicchio, A.; Lanfredi, A. M. M.; Bigoli, F. *Acta Crystallogr.* **1969**, *B25*, 354.

(36) Downing, H. D.; Williams, D. J. *J. Geophys. Res.* **1975**, *80*, 1656.

(37) Devlin, J. P.; Sadlej, J.; Buch, V. *J. Phys. Chem. A* **2001**, *105*, 974.